Numerical model of ice mélange expansion during abrupt ice-shelf collapse

Nicholas Guttenburg[1], Dorian S. Abbot[2], Jason M. Amundson[3], Justin C. Burton[1], L. Mac. Cathles[2], Douglas R. MacAyeal[2] and Wendy W. Zhang[1]

[1] *Department of Physics, University of Chicago, 5720 S. Ellis Ave., Chicago, IL, 60637, USA.*

[1] *Department of the Geophysical Sciences, University of Chicago, 5734 S. Ellis Ave, Chicago, IL 60637, USA.*

[3] *Geophysical Institute, University of Alaska, Fairbanks, AK, 99775, USA.*

Corresponding author: D. R. MacAyeal, E-mail: drm7@uchicago.edu

Authors following the first author are listed in alphabetical order.

ABSTRACT. The immediate residue of ice-shelf collapse along the Antarctic Peninsula is in many examples a large mass of small ice-shelf fragments (icebergs) that are oriented 90° from the initial firn-side-up 'life position' held while integrated within the ice shelf prior to its collapse. The overwhelming implication of this post-collapse arrangement is that iceberg capsize (with attendant gravitational potential energy release) is an important driver that accounts for the extraordinary damage and speed associated with ice-shelf collapse. To examine this implication, we construct a numerical model, featuring discrete particle elements, to study the kinematics and energy transfers that mediate the rapid expansion of ice-shelf fragments following the initiation of ice-shelf collapse (the ultimate cause of which is not a subject of study here). The model is highly idealized, 2-dimensional, and uses a simplified treatment of non-hydrostatic and free-surface effects of the ocean. The initial simulations derived from the model agree with phenomena observed in both Antarctic and Greenlandic examples of iceberg-capsize and fragmentation of floating ice in oceanic environments densely populated with ice mélange. This result augments the prevailing viewpoint that the ultimate trigger of ice-shelf instability along the Antarctic Peninsula is related to changing environmental conditions. The environmental change itself need not be the immediate driver of the incisive, chain-reaction associated with iceberg capsize that converts ice shelf or ice tongue into a chaotic ice mélange.

INTRODUCTION

Satellite imagery of the February 2008 Wilkins Ice-Shelf collapse reveals that a large percentage of the involved ice shelf was converted from integrated 'firn-side-up' ice shelf into a chaotic ice mélange consisting of small, capsized icebergs and broken iceberg fragments in less than about 24 hours (Scambos and others, 2009; Braun and Humbert, 2009; Braun and others, 2009).

Casual inspection of post-collapse satellite images of the Wilkins Ice Shelf (*e.g.,* the high-resolution images posted on the NSIDC website, `http://nsidc.org/news/images/20080325_wilkins_figure3.jpg`) suggest that much of the post-collapse arrangement of icebergs has little to do with the long-term stress regime associated with the ice shelf's gravitationally driven creeping flow prior to its collapse (see also, MacAyeal and others, 2003). The arrangement and fracture patterns of the post-collapse icebergs reveals an extreme degree of damage typically seen only in other ice-shelf collapse events, such as the Larsen B Ice Shelf in 2002, and in the break up of floating ice in Greenland fjords fed by fast-moving outlet glaciers (Howat and others, 2010; Amundson and others, 2010). A majority of fracture patterns seen in the imagery seem to be 'non-glaciological' in origin, *i.e.,* their orientations, geometries, separation scales and the lack of continuity from one iceberg to others that were neighbors while incorporated in the original ice shelf suggest a stress-loading process that operates on the scales of ocean waves, iceberg-capsize generated tsunamis, and iceberg-on-iceberg collisions in a fast-moving, outward expanding ice mélange.

The considerable amount of gravitational potential energy released when unstable icebergs capsize, offers a clue into what might be the important energy source controlling the extraordinary violence of ice-shelf collapse, as well as the non-glaciological patterns of iceberg fracture. As has been observed (e.g., Amundson and others, 2008; Nettles and others, 2008) in both Antarctic and Greenlandic settings, iceberg capsize generates tsunamic (impulsive) surface gravity wave energy that can subsequently stimulate the calving of new icebergs (MacAyeal and others, 2009, under review), the fragmentation of existing icebergs via collisions and flexure, and the capsize of conditionally unstable icebergs,*i.e.,* icebergs that can capsize only if given an initial nudge from some other process such as rocking induced by surface waves in the surrounding ocean (Bromirski and others, 2010, e.g.,).

While the perspective on ice-shelf collapse gleaned from post-collapse satellite imagery suggests immediate, proximal causes that reflect the interplay between the energy of capsizing icebergs, tsunamic impulses in the ocean and the stress effects of short-term hydrodynamic loading, it is essential to realize that ice-shelf collapse is primarily a climate-change phenomena (*e.g.,* as initially articulated by Mercer, 1978). So far, the only ice shelves to have collapsed are those located in regions of Antarctica (the peninsula) that exhibit a strong degree of secular warming over the past 25 years attributed to, among other things, increasing levels of atmospheric greenhouse gasses. Climate change, by mechanisms still under debate, appears to be the ultimate cause of ice-shelf collapse that unleashes the self-reinforcing, runaway iceberg capsize mechanism aluded to above. Free surface water, either openly visible in surface ponds connected with through piercing crevasses (Scambos and others, 2000), or invisibly held as brine within snow layers (Scambos and others, 2009), that associates with climate warming has been proposed as a possible enabling condition capable of producing the initial fragments of the ice shelf that can begin the runaway capsize process. Basal melting, which changes the relative depth of penetration of surface crevasses, has also been proposed as an environmental enabling condition (Shepherd and others, 2003).

Regardless of the ultimate enabling condition for ice-shelf collapse, the development of an understanding of the proximal, immediate drivers of ice-shelf fragmentation is necessary to comprehend the overall stability of ice shelves. Indeed, we can surmise, without advance knowledge of what the ultimate enabling condition may be, that parameters and geometries favorable to initiation of the iceberg-capsize process will be the primary avenue by which external environmental parameters, such as climate warming, will induce ice-shelf instability.

To investigate this suggestion, we present here preliminary versions of an idealized, 2-dimensional model of a disintegrating ice shelf composed of a large number (N$\sim$ 100 to $\sim>$ 1000) of initially closely packed icebergs of rigid body rheology and rectangular cross section. The fractures which separate the icebergs in the initial state are assumed to pre-exist, as we do not examine directly the process that induces initial fracture of the ice shelf into the pieces that subsequently capsize. The

model geometry and physical assumptions are idealized to an extreme degree as a means of gaining two advantages. First, we wish to study the most simple expression of the iceberg-capsize instability as the starting point for more advanced models to be developed in the future. Second, we design our model around the simple 'domino' geometry that is easily created in the laboratory, *e.g.* as shown in panel a of Figure (1) and in a companion presentation (Burton and others, unpublished talk presented at this symposium). The goal of this paper is to present details of the model construction and to illustrate the key model behavior that gives the model physical relevance to the ice-shelf collapse process: a feedback between iceberg capsize and ice mélange expansion across the ocean surface, as is witnessed in many collapse events.

MODEL DESIGN

The model domain is 2-dimensional and consists of a longitudinal cross section of the idealized ice mélange from a grounding line (or the upstream extent of ice-shelf fragmentation) to seaward ice front where the first iceberg meets the open ocean, and includes the region beyond the initial ice front to cover the open, ice-free water into which the collapsing ice mélange expands. The ice mélange is initially treated as a tightly packed sequence of rectangular, 'domino-like' icebergs of uniform dimensions and which are initially configured in a gravitationally unstable position (thickness greater than width). The seawater in which the icebergs float is treated as a hydrostatic fluid with a permanently undisturbed free surface, so that the complexities of free-surface waves can be eliminated for initial study. The interactions among the icebergs and between the icebergs and the water are assumed to be frictionless, except for a linear drag law resisting horizontal iceberg motion that is designed to simplify the dissipative effects of viscous forces and surface-gravity-wave radiation.

It is worth remarking that the geometry of our initial simulations is similar to a row of balanced dominoesVan Leeuwen (2004). However, unlike a row of dominoes, the domino-like icebergs in our simulations are afloat and are unstable to infinitessimal tilt perturbations (depending on the aspect ratio), whereas dominoes are initially stable standing on their short side, and only tip over when they experience a sufficient tipping force.

Each iceberg denoted by the index i has 3 degrees of freedom represented by the horizontal and vertical position of the center of mass (center of total area), x_i and z_i respectively, and by the angle of tilt, θ_i, measured counterclockwise with $\theta_i = 0$ implying that the iceberg is upright in the initial orientation when incorporated as part of the undisturbed ice shelf. Horizontal and vertical dimensions are rendered non-dimensional by scaling the system using the initial iceberg width, w, which is assumed to be less than the initial iceberg thickness, l. For each iceberg, the forces of gravity, buoyancy, and contact forces are resolved and used to compute linear and angular accelerations $\ddot{x}_i$, $\ddot{z}_i$, and $\ddot{\theta}_i$. These accelerations are used to compute velocities (both linear and angular) which are then stepped forward through time, using finite differencing, to determine the location and arrangement of the icebergs.

Four basic forces operate on each iceberg, 2 of which are depicted in panel b of Figure (1). Gravitational and buoyancy forces, F_g and F_b, respectively, are computed in the normal fashion from the total area of the iceberg (uniform density is assumed) and the area of the iceberg that is submerged below the sea surface. The sea surface is assumed to be undisturbed by waves, and hydrostatic pressure is assumed throughout the fluid that supports each iceberg. Contact forces, F_n, between neighboring icebergs are computed by considering instantaneous pairwise collisions that are partially elastic, as depicted in panel c of Figure (1). For collisions, those that will occur during a given timestep are identified, and impulses are calculated on pairwise sets of touching blocks so as to conserve both momentum and angular momentum, and to dissipate an amount of energy consistent with the coefficient of restitution of the ice (a parameter that determines the inelasticity of collisions).

A fourth force, a viscous damping term, is added both to the rotational dynamics and the translational dynamics in order to

model the loss of energy to the surrounding water in a generalized way. In this model we do not capture energy transfer between icebergs through waves. We model the viscous damping as an opposing force proportional to the translational velocity, and an opposing torque proportional to the angular velocity. We find that a value of the viscous dissipation constant of proportionality 0.01 (dimensionless) captures the appropriate decay timescale of the collective motion of fjord-bound ice mélange reported by (Amundson and others, 2010).

The dissipation term in our simulation is highly simplified. This is because at this stage of modelling we want to extract energy from the system in order to allow the icebergs to settle into a low-energy state on realistic timescales, but we are not yet concerned with the detailed trajectory of individual icebergs as they capsize. One could consider more accurate schemes to refine the model. Currently we do not consider a different degree of dissipation between submerged and exposed parts of the iceberg, nor do we take into account the cross-sectional area of the iceberg in the direction of motion. Eventually we intend to capture the interaction between a moving water surface and the icebergs, at which point these refinements will be implemented.

Gravity and Buoyant Forces

Each iceberg element has two body forces that act upon it continuously: the gravitational force which operates at the center of mass, and the buoyant force which operates at the center of buoyancy. These forces lead to an energy-minimizing orientation with respect to the surface of the liquid in which they float (for an example in other geophysical problems see (Collins and others, 2000)). We take the center of rotation of the iceberg elements to be their center of mass. In this way, gravity forces act downward at the center of mass of the element and do not contribute a torque to the rotational dynamics. The mass of each element is based on its volume and on the density of ice ρ_i, which is assumed uniform.

The force and torque (about the center of mass) contributions from buoyancy, F_b and τ_b, respectively, are evaluated using a volume integral over the submerged portion of the iceberg element:

$$\vec{F_b} = \int\int dxdz - (\rho_w - \rho_i) z\hat{z} \tag{1}$$

$$\tau_b = \int\int dxdz - (\rho_w - \rho_i) \frac{1}{2} xz \tag{2}$$

These contributions are consistent with a single force with magnitude $|F_b|$ acting in the $+z$ direction at the center of buoyancy, which is the center of area of the submerged portion of the iceberg. We compute these integrals by first representing our icebergs as four line segments whose equations we can determine based on the iceberg's rotation from the vertical. We iterate through each line segment, computing its intersection with the water surface to determine if it is entirely above water, below water, or crossing the water surface. We take only the portions that are below the water surface and, taking into account the direction of integration, evaluate the torque and buoyancy integrals as depicted in panel b of Figure (1). We remark that this method generalizes to model the buoyant force and torque upon any polygonal shape from a flat water surface.

Contact Forces

While we use timestepping to evaluate the dynamics of the icebergs under gravity and buoyancy, contact forces are extremely short-duration and large magnitude by comparison. There are two ways used to model contact forces in rigid body dynamics. One method involves allowing the individual bodies to be slightly compressible, and assigning a very stiff potential to the overlap between pairs of bodies, as used in (Pournin, 2005; Pöschel and Buchholtz, 1993) and many others. The other method

is to treat each collision as instantaneous and to use conservation laws to determine the velocities of the rigid bodies leaving the collision directly as used in (Hoomans and others, 1996).

We utilize the second method and treat collisions between icebergs as discrete events that transfer momentum and angular momentum through instantaneous impulses. To distinguish from the moment of inertia I we refer to this impulse as F_n, though it is an impulse rather than a force. In order to evaluate the contact impulse between a pair of colliding objects, we must assure that momentum and angular momentum are conserved, and that the kinetic energy of the icebergs after collision KE_f is proportional to the initial kinetic energy KE_i according to the (dimensionless) coefficient of restitution ϵ: $KE_f = \epsilon KE_i$. We restrict our consideration to a normal contact force (hence, use the subscript n on F_n), and so do not model either tangential restitution or microscopic friction between the icebergs.

In order to evaluate the contact normal force we need only know the positions of the icebergs' centers of mass, the position and surface normal at the collision point, and the linear and angular velocities of the two icebergs as shown in panel c of Figure (1). We must take into account that the contact points are moving both due to translational momentum and the rotations of the objects. The relative motion of the 2 colliding objects, denoted by labels 1 and 2, at the contact point is:

$$\vec{v_{1,2}} = (\vec{v_1} + \vec{r_1} \times (\omega_1 \hat{y})) - (\vec{v_2} + \vec{r_2} \times (\omega_2 \hat{y})) \tag{3}$$

The post-collision velocities are expressed in general in (Hahn, 1988) as a function of the coefficient of restitution ϵ such that $KE_f = \epsilon KE_i$:

$$\vec{v_{1,2}}' = -\epsilon \vec{v_{1,2}} \tag{4}$$

If we express all of the post-collisional velocities with respect to a collisional impulse acting along the normal direction F_n then we can solve for the normal impulse:

$$F_n = \frac{(1+\epsilon)\vec{v_{1,2}} \cdot \hat{n}}{\mu} \tag{5}$$

where

$$\mu = \frac{1}{m_1} + \frac{1}{m_2} + \frac{r_1^2}{I_1} + \frac{r_2^2}{I_2} \tag{6}$$

is a reduced mass. If this impulse is negative, it implies that the collision in question is due to numerical error introducing an overlap between receeding icebergs. For any such unphysical collisions we set the normal impulse to zero.

Collision Detection

Collisions between icebergs are handled computationally using techniques common to typical discrete particle mechanics codes used for the study of sand flows and other phenomena (e.g., Rycroft and others, 2009). Originally we used a sharp rectangular representation of the icebergs to detect collisions by determining when corners of the iceberg were inside other icebergs, or when pairs of lines between two icebergs intersected. We found that this collision representation introduced instabilities around the corners as it was possible that small errors caused the collision point and normal to be detected on the wrong side of the iceberg overlap, leading to collisions that pulled the icebergs together rather than pushing them apart.

In order to resolve this issue, and in anticipation of our eventual interest in treating icebergs that are not perfectly rectangular, it was necessary to round off the exterior of the icebergs. The simplest collision detection is that which considers pairs of discs or

spheres. Overlapping discs have been used to generate efficient bounding surfaces for collision detection between non-spherical particles (Donev and others, 2005). We take this a step further and entirely represent each rectangular iceberg by a series of overlapping discs. The discs are evenly divided between the four faces of the iceberg, and are evenly arrayed along each face as shown in panel d of Figure (1). This representation does not translate to the buoyancy calculations or the determination of the iceberg moment of inertia - it is used only to determine when and where icebergs come into contact. From that point, the contact forces can be determined without reference to the disc-representation of the collision volume. It is important to emphasize that the representation of icebergs using the discs is used only to detect collisions and to determine the direction of normal forces associated with collision. Buoyancy and other forces are computed using the exact rectangular geometry.

In order to speed up the check for collisions, we sort the icebergs into the cells of a grid underlying the simulation space whose dimensions are such that all collisions between icebergs will occur in the same or neighboring grid cells. We then use this to generate a list of potential collisions. For pairs of elements in this list, we check all pairs of discs comprising the iceberg against each other to detect whether there is a collision. If there is a collision, the collision location and surface normal (based on the disc geometry) are passed to a function that computes the normal impulse and evaluates the change in velocity and angular velocity. When a pair of icebergs collide there is an overlap on the order of $v\Delta t$ introduced due to the discrete timestepping we use, where v is the closing velocity and Δt is the time step size. In order to resolve this overlap, we move a colliding pair of icebergs back from their collision point until they are just touching. This ensures that icebergs do not get trapped in contact with each other through artificial penetration from the overlap. This method can introduce other collisions with neighboring icebergs, which then propagate stresses along the packed iceberg chain. The nature of the error introduced is that of a spurious compression wave whose wave speed is approximately the dimensions of an iceberg divided by the timestep size. We control for the error introduced by this spurious wave by varying the timestep until the simulation results do not depend on the timestep. Generally the error produced by this method is worst in configurations locked in place under compressive loading, which is not the case in our simulation as icebergs are free to leave from the edge of the collapsed ice sheet.

We must be careful of our representation as we explore icebergs with large aspect ratios. If the longest side of one of our icebergs is of length l and the discs forming its representation are of radius r_d then we must ensure that the discs actually do overlap to prevent holes from forming in our representation. If our representation has n_d discs per iceberg then the spacing between disc centers on the long side is $\frac{l}{n_d/4+1}$. We must ensure that this is no greater than $2r_d$. It is also worth considering that the further apart the discs are in the representation, the rougher that side of the iceberg is. This means that we have an effective friction due to the macroscopic roughness of our representation, albeit based on our numerical implimentation of collision detection. It is realistic for icebergs to have macroscopic roughness, but we must be careful to control for this effect so that we eventually understand any unphysical aspects of model behavior. To this end, we perform simulations that use 12-, 28- and 60-disc representations.

Initial Conditions

We initialize our simulations with 400 blocks of uniform aspect ratio (ratio of initial vertical dimension to initial horizontal dimewnsion of the rectangular icebergs, with aspect ratio greater than one signifying an initial width that is smaller than initial thickness) $\alpha = \frac{l}{w} = 1.4$ oriented vertically with random small perturbations in their angle to initiate the collapse. The randomness of the initial small perturbations introduces differences in the evolution of the experiments as times proceed, and these differences are evaluated (see below) to develop notions of fluctuation and uncertainty. The icebergs are initially stacked against the leftmost boundary of the simulation, which is treated as a rigid wall representing either the ice at the grounding line or the leading front of the remaining unfragmented ice shelf. The icebergs are stacked such that there is a gap of 0.1 iceberg

widths (simulation units) between them, to allow for the initial angular perturbations. Icebergbs can capsize and flow freely to the unoccupied right side of the model domain. We place the icebergs so that they are initially in hydrostatic equilibrium to avoid giving the system a large initial bobbing motion.

We define the dimensionless simulation variables by using the timescale $\tau = \sqrt{w/g}$ where w is the width of the icebergs and g is the gravitational acceleration. For icebergs 100 meters tall and 70 meters wide, one simulation time unit corresponds to 2.7 seconds. The system is allowed to evolve for 8000 simulation time units, corresponding to six hours. Our timestep is 0.01 time units, which is found to be the largest timestep that gives consistent results. The limiting factor for this choice of timestep is the stability of the buoyant oscillations, which grow in energy if the timestep is too large. For our material parameters we take the coefficient of restitution to be 0.5 and the viscous damping to be 0.01. This gives an exponential decay of the activity of the disintegrating ice sheet that is consistent with the decay of seismic signals observed in ice mélange of some Greenland fjords (Amundson and others, 2010).

RESULTS

The initial results of our simulations are reported here as a means of evaluating the utility of our numerical approach and assumptions. The results presented here are thus limited to basic qualitative phenomena, such as basic flow styles and time-scales of motion, leaving analysis of higher-order quantities such as pertaining to rates of energy conversion, seismic signals emanating from ice-mélange flows, and sensitivity to parameters such as iceberg aspect ratio to future study.

We observe two modes of 'collapse' of the initial, ordered iceberg arrangement. At short times, icebergs capsize everywhere where there is initial space to do so, including within the bulk of the ice mélange. However, once this initial instability is complete, the only way for the icebergs to capsize is for the ice mélange to expand. This occurs via the spreading of a phalanx of capsized icebergs at the edge of the mélange across the open ocean (Fig. 4). As the sheet expands, the rate at which icebergs capsize slows down and the system undergoes a period of evolution in which the rate of capsize and the rate of mélange advance into the open ocean proceed in a steady state. Eventually, once all the icebergs have capsized, the mélange stops moving as a result of the artificial dissipative effects we introduce (above), and the simulation is stopped.

We plot the fraction of icebergs that have capsized by at least 45° as a function of time in Figure (3), and also the position of the leading edge of the ice mélange as a function of time in Figure (4). Both figures display error bars, which represent the expected fluctuation associated with the randomness of initial tilt perturbations given as an initial condition to the ice mélange. Each figure also displays 3 curves representing sensitivity to the number of discs used in the representation of iceberg geometry needed for collision detection. Figure (5) depicts the local fractional density of capsized icebergs as a function of scaled position within the ice mélange as a function of time.

The evolution of the fraction of icebergs that have capsized as a function of time (Fig. 3) shows an initial period of rapid growth, corresponding to the initial capsize of icebergs that are surrounded by sufficient space to complete a rotation without having to significantly push surrounding ice mélange aside. This initial evolution decays into a steady state after about $t = 1000$, signifying the new physical dynamic that represents a one-to-one relationship between iceberg capsize and the seaward expansion of the ice mélange needed to make space for the capsized icebergs. This rapid growth of the fraction of icebergs capsized, followed by a steady state seems to correspond qualitatively with the evolution of both the Larsen B and Wilkins ice-shelf collapse events. In both cases, the first appearance of blue-colored (hence capsized or broken fragments) ice mélange grew very quickly in the wake of initial calving of a few icebergs that constituted the seaward leading edge of the subsequent mass of ice mélange (Scambos and others, 2009; Braun and Humbert, 2009; Braun and others, 2009). A

notable result of the simulations that was not anticipated from the limited observations of ice-shelf collapse is the fact that iceberg capsize evolves into a lengthy period of steady state evolution (prior to the end-game, when the collapse approaches completion) after an initially 'explosive growth' in the fraction of icebergs capsized. The fact that this period of steady state evolution exists, and the parameters that control its duration, can be studied in both simulations and observations for further understanding of the ice-shelf collapse dynamics.

In step with the fraction of capsized icebergs, the evolution of the position of the leading edge of the ice mélange as a function of time (Fig. 4) shows an initial period of rapid expansion, corresponding to the initial capsize of icebergs, followed by a period of relatively steady expansion into the open ocean needed to make room for the steady state growth in the fraction of icebergs that have capsized. Notable in this view of the system is the fact that a great deal of simulation to simulation variability (denoted by larger error bars) exists in the $t < 2000$ time period. This initial perod of variability is also reflected in the comparison of simulations that involve different numbers of discs used to detect collisions, where greatest sensitivity is seen in the initial $t < 2000$ period. Often in these simulations the leading iceberg is catapulted ahead by the collective flipping of the icebergs behind it. Thus, a large amount of energy is focused into the iceberg representing the furthest extent of expansion. The precise amount depends on which way each initial iceberg decides to flip, something that is very sensitive to the random tilt perturbations given to the initial arrangement of icebergs at the start of the simulations. At longer times, these effects are smeared out as the rest of the ice sheet catches up with the frontmost iceberg.

CONCLUSION

We have described an initial approach to simulating the ice mélange dynamics associated with collapsing ice shelves as recently witnessed along the Antarctic peninsula. The reasonable qualitative plausibility of the initial simulations presented above gives encouragement to the notion that it is possible to investigate the dynamics of the very short-time-span phenomena associated with explosive ice-shelf collapse using numerical simulation. What is missing, of course, is a definitive set of observations, both of a qualitative and quantitative nature, to which simulations of explosive ice-shelf collapse and the subsequent evolution of the ice mélange plume left in its wake can ber compared. We thus encourage future efforts to monitor any future collapse events with instruments and methods capable of discerning the various stages of evolution that may be compressed into the short hours-to-days long period.

We additionally note that our work illuminates only one aspect of the relatively speculative process that converts a pre-collapse ice shelf into the field of broken ice-shelf fragments typically resulting from climate-enabled ice shelf collapse. The physics represented in our model formulation does capture the most important mechanical energy source that drives the collapse after it begins, the latent gravitational energy of the unflipped icebergs. There is evidence that wave motion may be important in establishing how and when this energy is released, and so future work to capture the ice-water interaction is planned. Furthermore, the initial conditions of how the ice sheet breaks up can greatly change the timescales and eventual fate of the expanding ice sheet. These conditions originate in the processes which initially fragment the ice shelf into icebergs that have a geometry suceptible to capsize. As such, a deeper understanding of the physical mechanisms behind the initial breakup of the ice shelf is called for.

ACKNOWLEDGMENTS

This work is is supported by the US NSF under grants ANT-0944193, OPP-0838811 and CMG-0934534. D.S.A. was supported by the T. C. Chamberlin Fellowship of the University of Chicago and the Canadian Institute for Advanced Research.

References

Amundson, J. M., M. Fahnestock, M. Truffer, J. Brown, M. P. Lüthi and R. J. Motyka, 2010. Ice mélange dynamics and implications for terminus stability, Jakobshavn Isbræ, Greenland, J. Geophys. Res, **115**, F01005.

Amundson, J. M., M. Truffer, M. P. Lüthi, M. Fahnestock, M. West and R. J. Motyka, 2008. Glacier, fjord, and seismic response to recent large calving events, Jakobshavn Isbræ, Greenland, Geophys. Res. Lett, **35**, 22.

Braun, M. and A. Humbert, 2009. Recent retreat of Wilkins Ice Shelf reveals new insights in ice shelf breakup mechanisms, IEEE Geoscience and Remote Sensing Letters, **6**(2), 263–267.

Braun, M., A. Humbert and A. Moll, 2009. Changes of Wilkins Ice Shelf over the past 15 years and inferences on its stability, The Cryosphere, **3**, 41–56.

Bromirski, P. D., O. V. Sergienko and D. R. MacAyeal, 2010. Transoceanic infragravity waves impacting Antarctic ice shelves, Geophys. Res. Lett., **37**.

Collins, G., J. Head III, R. Pappalardo and N. Spaun, 2000. Evaluation of models for the formation of chaotic terrain on Europa, J. Geophys. Res, **105**, 1709–1716.

Donev, A., S. Torquato and F. H. Stillinger, 2005. Neighbor list collision-driven molecular dynamics simulation for nonspherical hard particles. I. Algorithmic details, Journal of Computational Physics, **202**(2), 737–764.

Hahn, J. K., 1988. Realistic animation of rigid bodies, Proceedings of the 15th annual conference on Computer graphics and interactive techniques, ACM, 299–308.

Hoomans, B. P. B., J. A. M. Kuipers, W. J. Briels and W. P. M. Van Swaaij, 1996. Discrete particle simulation of bubble and slug formation in a two-dimensional gas-fluidised bed: a hard-sphere approach, Chemical Engineering Science, **51**(1), 99–118.

Howat, I. M., J. E. Box, Y. Ahn, A. Herrington and E. M. McFadden, 2010. Seasonal variability in the dynamics of marine-terminating outlet glaciers in Greenland, J. Glaciol., **56**(198), 601–613.

MacAyeal, D.R., T.A. Scambos, C.L. Hulbe and M.A. Fahnestock, 2003. Catastrophic ice-shelf break-up by an ice-shelf-fragment-capsize mechanism, Journal of Glaciology, **49**(164), 22–36.

MacAyeal, D. R., D. S. Abbot and O. V. Sergienko, under review. Iceberg Tsunamis: Exploration of source mechanisms and hazard analysis using dimensional analysis, Ann. Glaciol., **58**.

MacAyeal, D. R., E. A. Okal, R. C. Aster and J. N. Bassis, 2009. Seismic observations of glaciogenic ocean waves (micro-tsunamis) on icebergs and ice shelves, J. Glaciol., **55**(190), 193–206.

Nettles, M., T. B. Larsen, P. Elósegui, G. S. Hamilton, L. A. Stearns, A. P. Ahlstrøm, J. L. Davis, M. L. Andersen, J. de Juan, S. A. Khan and others, 2008. Step-wise changes in glacier flow speed coincide with calving and glacial earthquakes at Helheim Glacier, Greenland, Geophys. Res. Lett, **35**.

Pöschel, T. and V. Buchholtz, 1993. Static friction phenomena in granular materials: Coulomb law versus particle geometry, Physical review letters, **71**(24), 3963–3966.

Pournin, L., 2005. On the behavior of spherical and non-spherical grain assemblies, its modeling and mumerical simulation, (Ph.D. thesis, École Polytechnique Fédérale de Lausanne.

Rycroft, C.H., A.V. Orpe and A. Kudrolli, 2009. Physical test of a particle simulation model in a sheared granular system, Physical Review E, **80**(3), 31305.

Scambos, T., H.A. Fricker, C.C. Liu, J. Bohlander, J. Fastook, A. Sargent, R. Massom and A.M. Wu, 2009. Ice shelf disintegration by plate bending and hydro-fracture: Satellite observations and model results of the 2008 Wilkins ice shelf break-ups,

Earth and Planetary Science Letters, **280**(1-4), 51–60.

Scambos, T.A., C. Hulbe, M. Fahnestock and J. Bohlander, 2000. The link between climate warming and break-up of ice shelves in the Antarctic Peninsula, Journal of Glaciology, **46**(154), 516–530.

Shepherd, A., D. Wingham, T. Payne and P. Skvarca, 2003. Larsen Ice Shelf has progressively thinned, Science, **302**(5646), 856–859.

Van Leeuwen, J. M. J., 2004. The Domino Effect, Arxiv preprint physics/0401018.

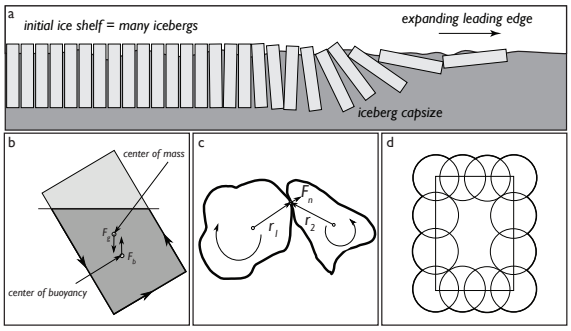

Fig. 1. Geometry of idealized ice mélange. (a) Conceptual model of the ice-shelf collapse process is depicted as a runaway capsize of a large mass of initially upright icebergs. Considerable gravitational potential energy is released by the capsize of each iceberg, and this energy drives seaward expansion of the leading ice mélange front. (b) The buoyant force on an iceberg is computed by determining the moments of the submerged portion of the iceberg. We do this by way of a contour integral around the boundary of the submerged portion. For each point on the boundary, we integrate from that point to the surface to compute the total buoyant force contributed by that column. By keeping the sign of the direction of integration, we subtract out all those parts that are submerged (such as in the overhang in this figure). The arrows show the direction of integration. (c) We compute the instantaneous impulse in a collision using the centers of mass and the contact point and surface normal. As long as we know these geometric factors and the incoming momenta we can determine the impulse F_n. (d) Our representation of the iceberg collision volume. This one uses 12 overlapping discs.

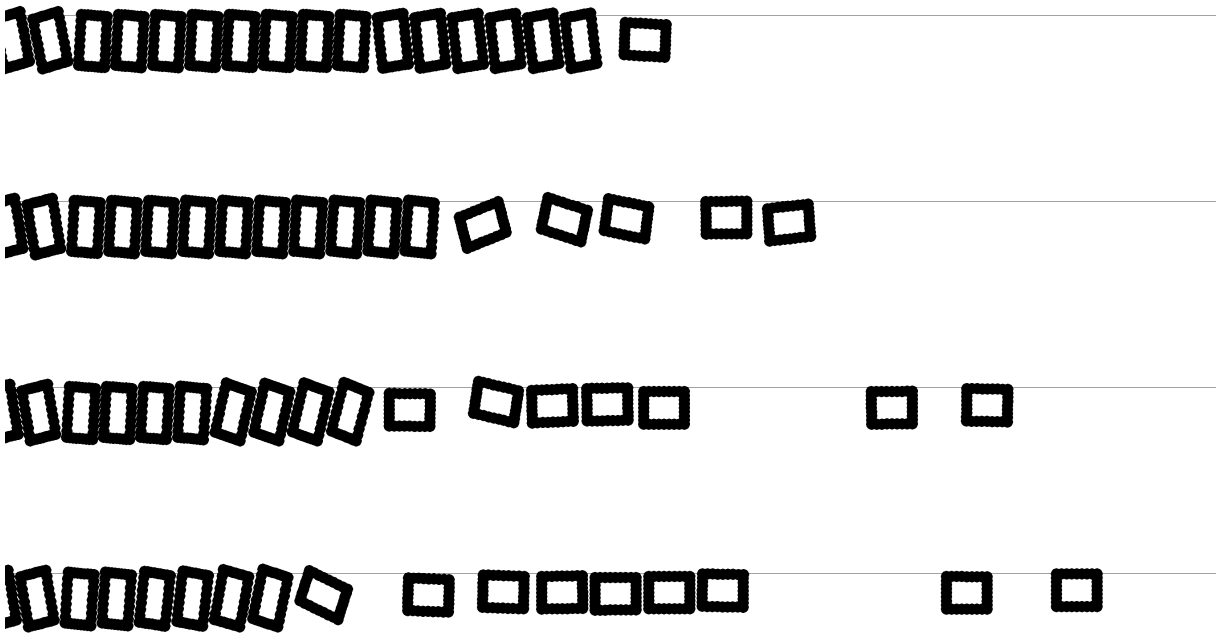

Fig. 2. This plot shows a view of the edge of the expanding ice mélange at times $t = 100$, $t = 200$, $t = 300$, and $t = 400$ (top to bottom). The representation of each iceberg as a series of overlapping discs is shown. The 28-disc representation was used for this sequence.

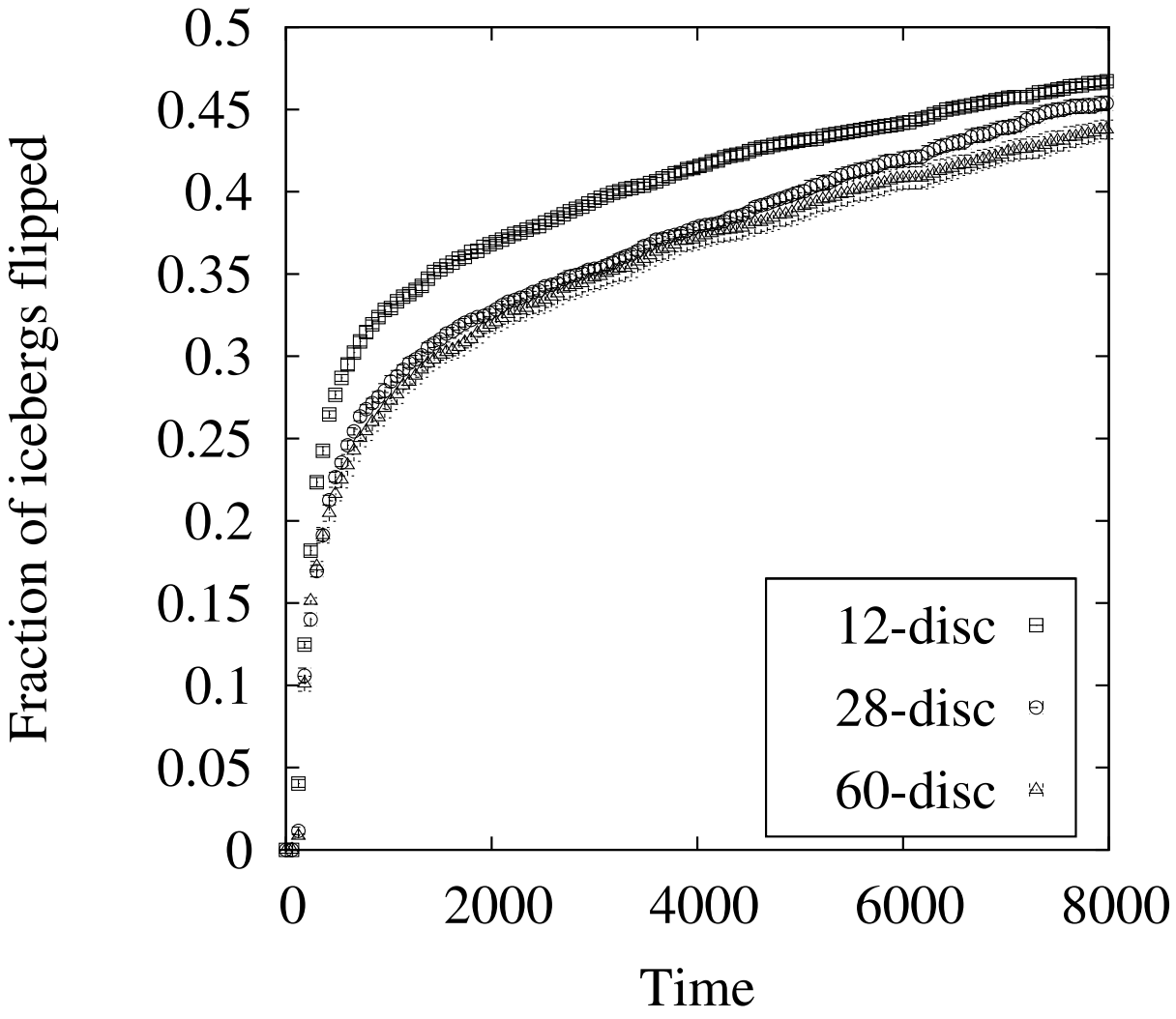

Fig. 3. This plot shows the fraction of icebergs caosuzed by at least 45° as a function of time for a 12-disc, 28-disc, and 60-disc representation. Each curve is averaged over eight simulation runs with different initial conditions. The error bars are determined from the standard deviation of the simulation results at each time.

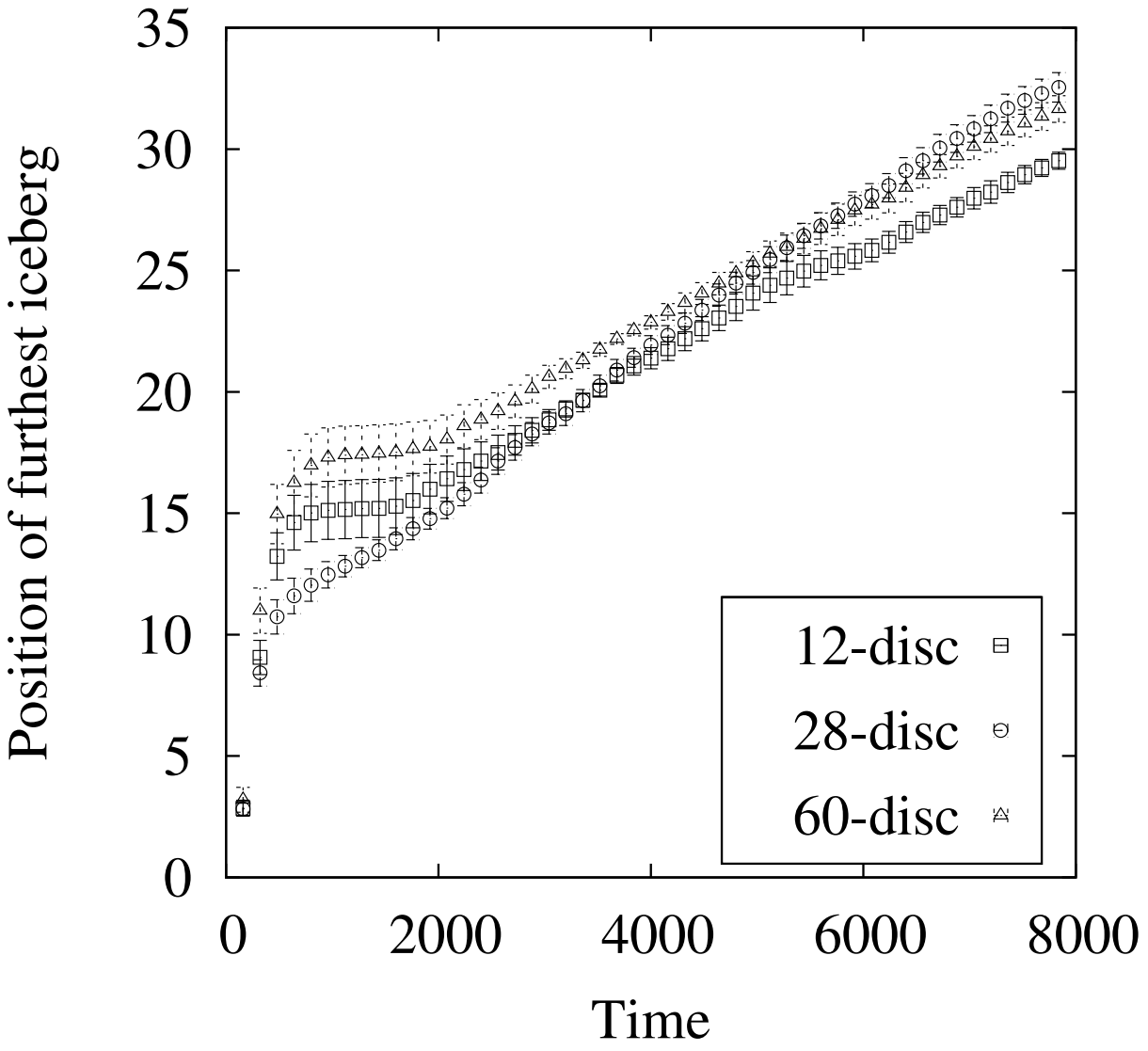

Fig. 4. This plot shows the position of the furthest iceberg (non dimensional units) from the ice shelf relative to its initial position, averaged over eight runs of the simulation with different initial conditions and error bars determined from the standard deviation of the simulation results. The 12-disc, 28-disc, and 60-disc results are each shown.

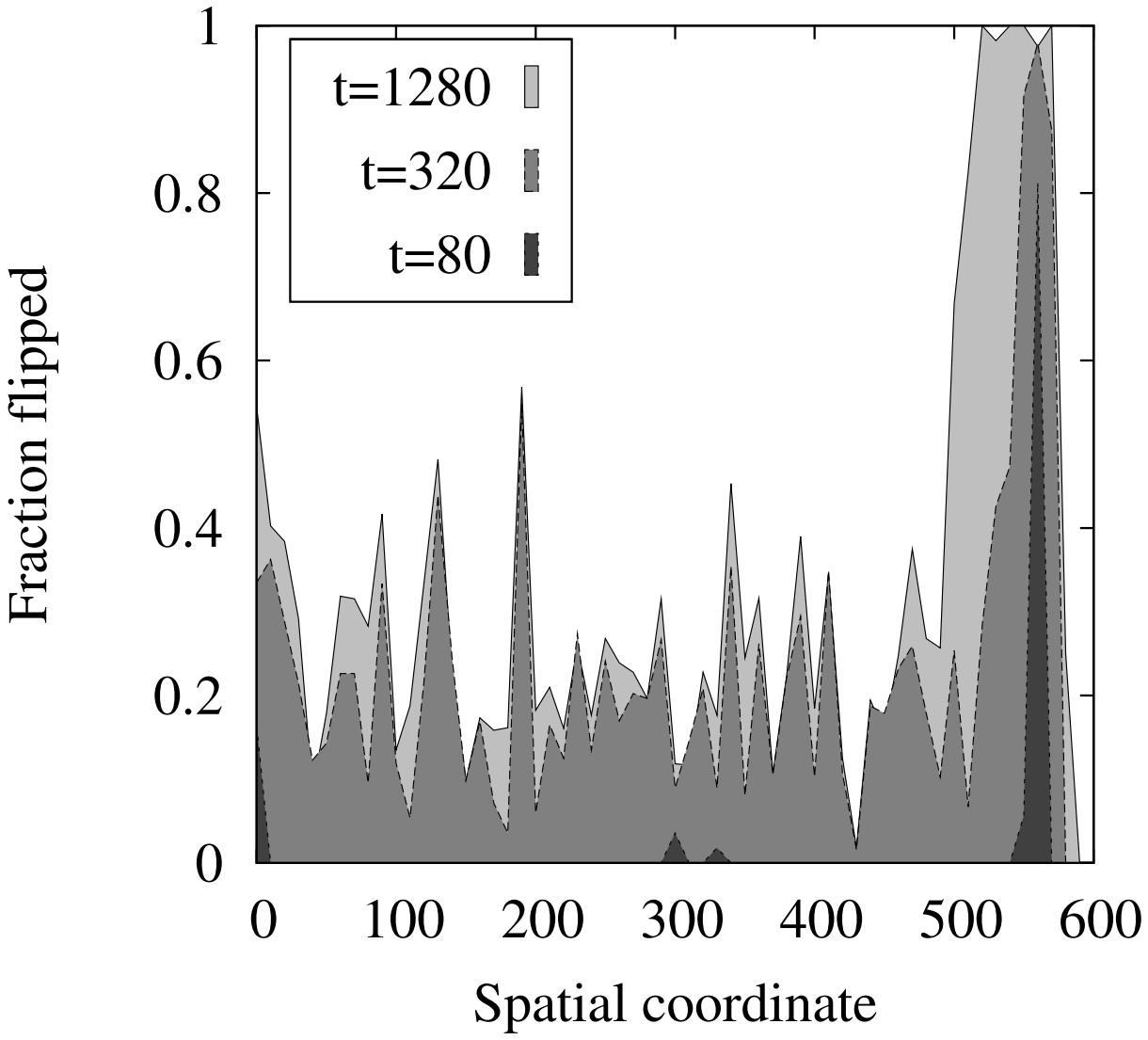

Fig. 5. The fraction of icebergs capsized as a function of the horizontal span of the ice mélange at various times during the ice shelf collapse. The phalanx of capsized icebergs at the expanding edge is visible. These results are averaged over eight simulation runs and over spatial regions 10 non-dimensional units in width. The results shown here are for the 60-disc representation.